



Development and Assessment of an Isotropic Four-Equation Model for Heat Transfer of Low Prandtl Number Fluids

Xingkang Su^{1,2}, Xianwen Li^{1,2}, Xiangyang Wang³, Yang Liu³, Qijian Chen³, Qianwan Shi³, Xin Sheng^{1,2} and Long Gu^{1,2,3*}

¹Institute of Modern Physics, Chinese Academy of Sciences, Lanzhou, China, ²School of Nuclear Science and Technology, University of Chinese Academy of Sciences, Beijing, China, ³School of Nuclear Science and Technology, Lanzhou University, Lanzhou, China

OPEN ACCESS

Edited by:

Wei Ding,
Helmholtz Association of German
Research Centres (HZ), Germany

Reviewed by:

Yacine Addad,
Khalifa University, United Arab
Emirates

Luteng Zhang,
Chongqing University, China

*Correspondence:

Long Gu
gulong@impcas.ac.cn

Specialty section:

This article was submitted to
Nuclear Energy,
a section of the journal
Frontiers in Energy Research

Received: 16 November 2021

Accepted: 14 January 2022

Published: 08 February 2022

Citation:

Su X, Li X, Wang X, Liu Y, Chen Q,
Shi Q, Sheng X and Gu L (2022)
Development and Assessment of an
Isotropic Four-Equation Model for Heat
Transfer of Low Prandtl Number Fluids.
Front. Energy Res. 10:816560.
doi: 10.3389/fenrg.2022.816560

In the simple gradient diffusion hypothesis, the turbulent Prandtl number (Pr_t) with a constant of 0.85 is difficult to accurately predict for liquid metals having low Prandtl numbers (Pr), while a four-equation model can improve this solution by introducing the turbulence time-scale into the calculation of turbulent thermal diffusivity. However, the four-equation model's transport form and numerical stability are so complex that suitable commercial code is lacking. Therefore, an isotropic four-equation model with simple Dirichlet wall boundary conditions is built in the present work. Based on the open-source computational fluid dynamics program OpenFOAM, the fully developed velocity, temperature, Reynolds stress, and heat flux of low Pr fluids ($Pr = 0.01-0.05$) in the parallel plane are obtained by numerical simulation. The results show that the time-average statistics predicted using the present four-equation model are in good agreement with the direct numerical simulation data. Then, the isotropic four-equation model is used to analyze the flow and heat of liquid metal ($Pr = 0.01$) in a quadrilateral infinite rod bundle. The numerical results are compared with the various and available experimental relationships. The Nusselt numbers calculated using the isotropic four-equation model are betweenness the available correlations, while the turbulent Prandtl number model using a constant of 0.85 over predicts heat transfer. More detailed local heat transfer phenomena and distribution of low Pr fluids are obtained using the present isotropic four-equation model.

Keywords: low Pr fluid, four-equation, OpenFOAM, heat transfer, liquid metal

1 INTRODUCTION

Liquid metals are widely considered coolants with good thermal-hydraulic characteristics for many energy systems, such as fast reactors and subcritical reactors (Gu and su, 2021; Wang et al., 2021). However, liquid metals' low molecular Prandtl number Pr leads to special heat transfer compared to traditional fluids. Typically, the Pr of lead-bismuth is 0.03–0.01 and that of sodium is 0.01–0.006 (Vià et al., 2020). It is significant to study liquid metals' turbulent heat transfer characteristics, which will affect the economy and security of the energy system.

It is difficult, dangerous, and costly to experiment with liquid metals (Schroer et al., 2012; Ejenstam and Szakálos, 2015), while the computational fluid dynamics (CFD) method is more commonly applied to investigate the thermal-hydraulic properties of these liquids. However, in CFD, the computing cost required by the direct numerical simulation (DNS) method and the large eddy simulations (LES) method is too high to rely on this technique for a quick and economic calculation of heat transfer in complex geometries (Kawamura et al., 1999), while the Reynolds Averaged Navier–Stokes (RANS) method can be promoted. The velocity boundary layer and the temperature layer of traditional fluid ($Pr \approx 1$) are generally considered to be similar in the RANS framework. In this way, one can obtain a constant turbulent Prandtl number Pr_t to simplify the calculation of the energy equation after using the simple gradient diffusion hypothesis (SGDH) (Groetzbach, 2013). However, it is invalid for low Pr fluids (Reynolds, 1975).

In the SGDH framework, Cheng (Cheng and Tak, 2006) derived a Pr_t correlation through employing global Reynolds numbers, while Kays (Kays, 1994) introduced the local turbulence effect into the Pr_t relation. These nonlinear Pr_t relations can effectively improve this problem in some simple geometries. However, these relations still need to be further verified in complex geometries (Duponcheel et al., 2014). Unlike the SGDH method, the differential or algebraic heat flux model (D/AHFM) establishes differential or algebraic transport equations to consider the dissimilarity between velocity and the temperature field to improve the heat transfer accuracy of liquid metals. Assessment and calibration results of D/AHFM models for low Pr fluids completed in some simple geometries show that the heat transport of second-moment closure is very sensitive to the model coefficients and functions (Lai and So, 1990; Shikazono and Kasagi, 1996; Choi and Kim, 2007; Shams et al., 2019).

Another popular model in the SGDH work, called the four-equation k - ε - k_θ - ε_θ turbulent heat transfer model, is introduced into turbulent and thermal time-scales for the simulation of the explicit first-order turbulent heat diffusivity. The literature (Nagano and Kim, 1988; Abe et al., 1995; Nagano and Shimada, 1996) has contributed extensively to near-wall model closure and thermal turbulence effect for a four-equation model. In recent years, Manservisi (Manservisi and Menghini, 2014a) improved the four-equation k - ε - k_θ - ε_θ model proposed by Abe and Nagano. The model predicted the heat transfer process of the plane, circular tube, triangular rod bundles, and quadrilateral rod bundles for $Pr = 0.025$ fluids (Manservisi and Menghini, 2014b; Manservisi and Menghini, 2015). However, the numerical stability of the four-equation model is affected by its near-wall boundary conditions. To improve the problem, a four-equation k - ω - k_θ - ω_θ model with the specific dissipation rates $\omega = \varepsilon/(C_\mu k)$ and $\omega_\theta = \varepsilon_\theta/(C_\mu k_\theta)$ was developed based on Manservisi's k - ε - k_θ - ε_θ model (Cerroni et al., 2015). Then by the following work of the literatures (Vià et al., 2016; Chierici et al., 2019; Vià and Manservisi, 2019), logarithmic specific dissipation rates of ω and ω_θ , that is, $\Omega = \ln(\omega)$ and $\Omega_\theta = \ln(\omega_\theta)$, have been used to simplify the near-wall boundary conditions and have been

introduced into the logarithmic four-equation k - Ω - k_θ - Ω_θ model. Other state variables as proposed by Youssef (Youssef, 2006) are the velocity $\tau_u = k/\varepsilon$ and temperature time-scale $\tau_\theta = k_\theta/\varepsilon_\theta$ to improve its numerical stability. The proposed k_θ - τ_θ model does not suffer from numerical stiffness problems since natural boundary conditions for the variables k_θ and τ_θ are used ($k_\theta = \tau_\theta = 0$, at walls). In addition, the static variables $\tilde{\varepsilon}$ and $\tilde{\varepsilon}_\theta$, called the isotropic dissipation rates, which are linked to the “true” dissipation rates ε and ε_θ , can also provide Dirichlet wall boundary conditions and simpler transport modes than the k_θ - τ_θ modes (Nagano and Shimada, 1996; Nagano et al., 1997).

However, the application codes of an isotropic four-equation model in complex geometries are still lacking for liquid metals, and its reliability needs to be further verified and evaluated. So, in the present work, the four-equation model in an isotropic dissipation rate $k - \tilde{\varepsilon} - k_\theta - \tilde{\varepsilon}_\theta$ formulation for liquid metals to improve its numerical robustness was presented by Taylor series expansion and near-wall turbulence analysis based on Abe's model and Manservisi's model. The turbulent heat transfer process of $Pr = 0.01 \sim 0.05$ fluids in parallel planes is numerically studied based on the finite volume method and the open-source CFD program OpenFOAM. The validity of the present four-equation model was verified by DNS data. To evaluate the present model's applicability in complex geometries, the turbulent heat transfer of $Pr = 0.01$ fluids in a bare quadrilateral infinite rod bundle with different pitch-to-diameter ratios is predicted on the present isotropic four-equation model. The numerical results obtained from two SGDH options, the $Pr_t = 0.85$ model and the present isotropic $k - \tilde{\varepsilon} - k_\theta - \tilde{\varepsilon}_\theta$ model, are compared and analyzed with the available experimental relations and CFD results. The local distributions of dimensionless temperature, temperature fluctuation, turbulent heat diffusivity, and turbulent Prandtl numbers are analyzed.

2 MATHEMATICAL MODEL

2.1 Isotropic Four-Equation Turbulence Model

The incompressible RANS equations with no gravity and constant physical properties for the calculation of velocity, pressure, and temperature fields are considered as follows:

$$\frac{\partial u_i}{\partial x_i} = 0 \quad (1)$$

$$\frac{\partial u_i}{\partial t} + u_j \frac{\partial u_i}{\partial x_j} = -\frac{1}{\rho} \frac{\partial P}{\partial x_i} + \frac{\partial}{\partial x_j} \left(\nu \frac{\partial u_i}{\partial x_j} \right) - \frac{\partial}{\partial x_j} \overline{u'_i u'_j} \quad (2)$$

$$\frac{\partial T}{\partial t} + u_j \frac{\partial T}{\partial x_j} = \frac{\partial}{\partial x_j} \left(\alpha \frac{\partial T}{\partial x_j} \right) - \frac{\partial}{\partial x_j} \overline{u'_j T'} \quad (3)$$

where u_i , P , and T are the RANS velocities, pressure, and temperature fields. ν , ρ , and α are the molecular viscosity, density, and molecular thermal diffusivity, respectively. The Reynolds stress $\overline{u'_i u'_j}$ using the Boussinesq hypothesis and Reynolds flux $\overline{u'_j T'}$ using the SGDH are set as follows:

$$\overline{u'_i u'_j} = -\nu_t \left(\frac{\partial u_i}{\partial x_j} + \frac{\partial u_j}{\partial x_i} \right) + \frac{2k}{3} \delta_{ij} \quad (4)$$

$$\overline{u'_j T'} = -\alpha_t \frac{\partial T}{\partial x_j} \quad (5)$$

The turbulent viscosity ν_t can be solved using two-equation $k - \varepsilon$ or $k - \omega$ models, while the turbulent thermal diffusivity α_t is considered as follows:

$$\alpha_t = \frac{\nu_t}{Pr_t} \quad (6)$$

Due to low Pr fluids' physical properties, there are great differences between the momentum and heat. A constant $Pr_t \approx 0.85-0.9$ cannot give acceptable results for liquid metals. It is possible to consider α_t as a function of the turbulence variables, such as two-equation $k_\theta - \varepsilon_\theta$ or $k_\theta - \omega_\theta$ analogy to dynamic two-equation $k - \varepsilon$ or $k - \omega$. To smooth the isotropic variables at the wall, when one makes $\tilde{\varepsilon}$ and $\tilde{\varepsilon}_\theta$ zero at the wall, an isotropic four-equation $k - \tilde{\varepsilon} - k_\theta - \tilde{\varepsilon}_\theta$ model can be written using the Taylor series expansion as follows:

$$\tilde{\varepsilon} = \varepsilon - 2\nu(\sqrt{k_{,2}})^2 \quad (7)$$

$$\tilde{\varepsilon}_\theta = \varepsilon_\theta - 2\alpha(\sqrt{k_{\theta,2}})^2 \quad (8)$$

$$\frac{\partial k}{\partial t} + u_j \frac{\partial k}{\partial x_j} = \frac{\partial}{\partial x_j} \left[\left(\nu + \frac{\nu_t}{\sigma_k} \right) \frac{\partial k}{\partial x_j} \right] + P_k - \tilde{\varepsilon} - 2\nu \left(\frac{\partial \sqrt{k}}{\partial x_j} \right)^2 \quad (9)$$

$$\begin{aligned} \frac{\partial \tilde{\varepsilon}}{\partial t} + u_j \frac{\partial \tilde{\varepsilon}}{\partial x_j} = & \frac{\partial}{\partial x_j} \left[\left(\nu + \frac{\nu_t}{\sigma_\varepsilon} \right) \frac{\partial \tilde{\varepsilon}}{\partial x_j} \right] + C_{\varepsilon 1} \frac{\tilde{\varepsilon}}{k} P_k - C_{\varepsilon 2} f_\varepsilon \frac{\tilde{\varepsilon}^2}{k} \\ & + \nu \nu_t (1 - f_w) \left(\frac{\partial^2 u_i}{\partial x_j \partial x_k} \right)^2 \end{aligned} \quad (10)$$

$$\frac{\partial k_\theta}{\partial t} + u_j \frac{\partial k_\theta}{\partial x_j} = \frac{\partial}{\partial x_j} \left[\left(\alpha + \frac{\alpha_t}{\sigma_{k_\theta}} \right) \frac{\partial k_\theta}{\partial x_j} \right] + P_{k_\theta} - \tilde{\varepsilon}_\theta - 2\alpha \left(\frac{\partial \sqrt{k_\theta}}{\partial x_j} \right)^2 \quad (11)$$

$$\begin{aligned} \frac{\partial \tilde{\varepsilon}_\theta}{\partial t} + u_j \frac{\partial \tilde{\varepsilon}_\theta}{\partial x_j} = & \frac{\partial}{\partial x_j} \left[\left(\alpha + \frac{\alpha_t}{\sigma_{\varepsilon_\theta}} \right) \frac{\partial \tilde{\varepsilon}_\theta}{\partial x_j} \right] + C_{p1} \frac{\tilde{\varepsilon}_\theta}{k_\theta} P_{k_\theta} + C_{p2} \frac{\tilde{\varepsilon}_\theta}{k} P_k \\ & - C_{d1} \frac{\tilde{\varepsilon}_\theta}{k_\theta} \tilde{\varepsilon}_\theta - C_{d2} f_{d2} \frac{\tilde{\varepsilon}_\theta}{k} \tilde{\varepsilon} + \alpha \alpha_t (1 - f_{w\theta}) \left(\frac{\partial^2 T}{\partial x_j \partial x_k} \right)^2 \end{aligned} \quad (12)$$

$$P_k = -\overline{u'_i u'_j} \frac{\partial u_i}{\partial x_j}, P_{k_\theta} = -\overline{u'_j T'} \frac{\partial T}{\partial x_j} \quad (13)$$

$$f_\varepsilon = \{1 - 0.3 \exp[-(R_t/6.5)^2]\} \quad (14)$$

$$f_w = (1 - \exp(-R_\varepsilon/19))^2 \quad (15)$$

$$f_{d2} = 1/C_{d2} (C_{\varepsilon 2} f_\varepsilon - 1) [1 - \exp(-R_\varepsilon/5.7)]^2 \quad (16)$$

$$f_{w\theta} = (1 - \exp(-R_\varepsilon \sqrt{Pr}/19))^2 \quad (17)$$

where $\tilde{\varepsilon}$ and $\tilde{\varepsilon}_\theta$ call the isotropic dissipation rate. ε and ε_θ are the "true" dissipation rate, respectively. $f_\varepsilon, f_w, f_{d2}$, and $f_{w\theta}$ are wall-proximity effect functions. Based on the analysis of the literature and the DNS database (Abe et al., 1995; Kawamura et al., 1998; Manservisi and Menghini, 2014a), the isotropic four-equation model coefficients for liquid metals are used and corrected as

TABLE 1 | Values for the $k - \tilde{\varepsilon} - k_\theta - \tilde{\varepsilon}_\theta$ model constants in Eqs 9–12.

$C_{\varepsilon 1}$	$C_{\varepsilon 2}$	σ_k	σ_ε	C_{p1}	C_{p2}	C_{d1}	C_{d2}	σ_{k_θ}	$\sigma_{\varepsilon_\theta}$
1.5	1.9	1.4	1.4	0.925	0.9	1.1	0.9	1.4	1.4

shown in **Table 1**. Here, the $k - \tilde{\varepsilon} - k_\theta - \tilde{\varepsilon}_\theta$ model functions and constants recommended in this study, such as $f_\varepsilon, f_w, f_{d2}, f_{w\theta}$, and C_{d1} , are different from the $k - \varepsilon - k_\theta - \varepsilon_\theta$ model values of Manservisi (Manservisi and Menghini, 2014b). It is noted that P_{k_θ} is the production term of temperature fluctuations k_θ , which represents the energy transferred to the turbulent flux by the average temperature change rate of the RANS flow. That is, the temperature fluctuations k_θ is the result of the combined action of the average temperature change rate and Reynolds heat flux. Through the transport of **Eq. 11**, after the temperature fluctuation occurs, it will experience convection, molecular diffusion, and turbulent diffusion until it is dissipated.

Both the turbulent Reynolds number $R_t = k^2/\nu\varepsilon$ and R_ε are introduced into the isotropic model. Let δ be the wall distance. R_ε can be recommended by Abe et al. (Abe et al., 1995), as follows:

$$R_\varepsilon = \delta/\eta \quad (18)$$

where $\eta = (\nu^3/\varepsilon)^{1/4}$ is the Kolmogorov length scale which can calculate the separated flow well. When isotropic variables are used, R_t and R_ε in **Eqs 14–17** should become the following:

$$R_t = k^2/\nu\tilde{\varepsilon}, R_\varepsilon = \delta/\eta \text{ where } \eta = (\nu^3/\tilde{\varepsilon})^{1/4} \quad (19)$$

2.2 Turbulent Viscosity and Turbulent Thermal Diffusivity

Some dynamic and thermal time-scales should be applied to calculate the turbulent viscosity ν_t and turbulent thermal diffusivity α_t . Using dynamic and thermal time-scales, that is, $\tau_u = k/\varepsilon$ and $\tau_\theta = k_\theta/\varepsilon_\theta$, turbulent viscosity and turbulent thermal diffusivity can be defined (Abe et al., 1995; Manservisi and Menghini, 2015) as follows:

$$\nu_t = C_u f_u k \tau_u \quad (20)$$

where

$$f_u = \left\{ 1 - \exp\left(-\frac{R_\varepsilon}{14}\right) \right\}^2 \left(1 + \frac{5}{R_t^{3/4}} f_d \right) \quad (21)$$

and

$$f_d = \exp^{-(R_t/200)^2} \quad (22)$$

$$\alpha_t = C_\lambda f_\lambda k \tau_u \quad (23)$$

where

$$\begin{aligned} f_\lambda = & \left\{ 1 - \exp\left(-\frac{R_\varepsilon}{14}\right) \right\} \left\{ 1 - \exp\left(-\frac{R_\varepsilon \sqrt{Pr}}{19}\right) \right\} \\ & \left(Pr_{t\infty} + \frac{2R}{C_m + R} f_{\theta 1} + \frac{\sqrt{2R}}{Pr} \frac{1.3}{R_t^{3/4}} f_{\theta 2} \right) \end{aligned} \quad (24)$$

$$f_{\theta 1} = \exp^{-(R_t/500)^2} \quad (25)$$

and

TABLE 2 | Series expansion near the wall.

Mean parameter	Fluctuating parameter
$u = A_1\delta + A_2\delta^2 + A_3\delta^3 + \dots$	$u' = a_1\delta + a_2\delta^2 + a_3\delta^3 + \dots$
$v = B_2\delta^2 + B_3\delta^3 + \dots$	$v' = b_2\delta^2 + b_3\delta^3 + \dots$
$w = C_1\delta + C_2\delta^2 + C_3\delta^3 + \dots$	$w' = c_1\delta + c_2\delta^2 + c_3\delta^3 + \dots$
$T = D_1\delta + D_2\delta^2 + D_3\delta^3 + \dots$	$T' = d_1\delta + d_2\delta^2 + d_3\delta^3 + \dots$

$$f_{\theta_2} = \exp^{-(R_t/200)^2} \tag{26}$$

The above model has been proved to be effective in producing correct turbulence behavior of liquid metal, which draws into the mixing time-scale $\tau_m = \tau_u R / (C_m + R)$ and the ratio of the velocity time-scale to the thermal time-scale $R = \tau_\theta / \tau_u$ (Abe et al., 1995). The values of $Pr_{t\infty} = 0.9$ and $C_m = 0.3$ are recommended for liquid metals (Manservigi and Menghini, 2015). In order to establish a complete isotropic four-equation turbulent heat transfer model $k - \tilde{\epsilon} - k_\theta - \tilde{\epsilon}_\theta$, we used the isotropic variables $\tilde{\epsilon}$ and $\tilde{\epsilon}_\theta$ in Eqs 20–26 instead of the “true” variables ϵ and ϵ_θ .

2.3 Wall Boundary Conditions for Turbulence Models

Appropriate boundary conditions should be applied to solve the four-equation turbulent models without the available wall functions. By using series expansions as shown in Table 2, the near-wall behaviors of dynamical and thermal turbulence variables k , ϵ , k_θ , and ϵ_θ can be obtained (Deng et al., 2001) as follows:

$$\begin{aligned} k &= \frac{1}{2} \overline{u_i' u_i'} = \frac{1}{2} \overline{(a_i^2 + c_i^2)} \delta^2 + \dots \\ \epsilon &= \nu \frac{\partial u_i'}{\partial x_j} \frac{\partial u_i'}{\partial x_j} = \nu \left(\overline{a_i^2 + c_i^2} \right) + \dots = 2\nu (\sqrt{k_{\theta,2}})^2 + \dots \\ k_\theta &= \frac{1}{2} \overline{T' T'} = \frac{1}{2} \left(\overline{d_i^2} \right) \delta^2 + \dots \\ \epsilon_\theta &= \alpha \frac{\partial T'}{\partial x_j} \frac{\partial T'}{\partial x_j} = \alpha \overline{d_i^2} + \dots = 2\alpha (\sqrt{k_{\theta,2}})^2 + \dots \end{aligned} \tag{27}$$

According to the definitions of Eqs 7, 8, when δ tends to zero, k , $\tilde{\epsilon}$, k_θ , and $\tilde{\epsilon}_\theta$ tend to zero. Thus, the simple Dirichlet wall boundary conditions with the isotropic $k - \tilde{\epsilon} - k_\theta - \tilde{\epsilon}_\theta$ model can be imposed.

2.4 Modified Navier–Stokes Equations for Periodic Boundary Conditions

For a fully developed turbulent field, the pressure gradient term in Eq. 2 is divided into the mean of the pressure gradient dP_f/dz which is constant along the flow direction z and the fluctuating pressure gradient $\partial P/\partial x_i$. The mean term of the pressure gradient is given as the known power source term.

$$\frac{\partial u_i}{\partial t} + u_j \frac{\partial u_i}{\partial x_j} = -\frac{1}{\rho} \frac{\partial P}{\partial x_i} + \frac{1}{\rho} \frac{dP_f}{dz} + \frac{\partial}{\partial x_j} \left(\nu \frac{\partial u_i}{\partial x_j} \right) - \frac{\partial}{\partial x_j} \overline{u_i' u_j'} \tag{28}$$

TABLE 3 | Physical properties for $Pr = 0.01, 0.025, \text{ and } 0.05$

Parameter	Value	Unit	Symbol	Pr
Dynamic viscosity	0.00181	Pa·s	μ	—
Density	10,340	kg/m ³	ρ	—
Specific heat capacity	145.75	J/(kg · K)	C_p	—
Thermal conductivity	5.27615	W/(m · K)	λ	0.05
	10.5523	—	—	0.025
	26.38075	—	—	0.01

For a fully developed temperature field, temperature T is written as follows:

$$\theta(x, y) = T_{in} + z\Delta T_b - T(x, y, z) \tag{29}$$

where T_{in} is the inlet temperature, and ΔT_b is a constant wall temperature gradient, while θ satisfies periodic boundary conditions along the flow direction. According to the energy conservation for thermal fully developed flow with a wall flux q_w , ΔT_b can be set as $4q_w / (\rho C_p u_b D_h)$, where u_b is average velocity, and D_h is an equivalent diameter. After introducing periodic temperature θ , Eq. 3 can be written as follows:

$$\frac{\partial \theta}{\partial t} + u_j \frac{\partial \theta}{\partial x_j} = \frac{\partial}{\partial x_j} \left(\alpha \frac{\partial \theta}{\partial x_j} \right) - \frac{\partial}{\partial x_j} \overline{u_j' \theta'} + u_z \Delta T_b \tag{30}$$

3 NUMERICAL RESULTS AND ANALYSIS

3.1 Numerical Solver of the Isotropic Four-Equation Model

For the modified RANS system and the isotropic four-equation $k - \tilde{\epsilon} - k_\theta - \tilde{\epsilon}_\theta$ model in Section 2, the appropriate discrete format could be selected according to the needs. Here, the convection term adopts the Gauss upwind format, the diffusion term uses the Gauss linear format, and the time term uses the steady-state format. The SIMPLE algorithm solves the continuity and momentum simultaneously, and coupled multigrid iteration is used for the matrix solution. The convergence conditions of residual error are as follows:

$$\text{Max} \left| \frac{Q^{i+1}}{Q^i} - 1 \right| < 10^{-9} \tag{31}$$

where Q stands for u_i , θ , k , $\tilde{\epsilon}$, k_θ and $\tilde{\epsilon}_\theta$. The index i denotes the steps of calculation. All calculations were realized on OpenFOAM (Weller et al., 1998; Moukalled et al., 2016). The detailed analysis of the four-equation model solver by Gu and Su (Gu and su, 2021) based on OpenFOAM can be further referred to. The height of the grid point closest to the wall is approximately 10^{-3} mm to meet the requirements of the isotropic four-equation model ($y^+ < 1$).

3.2 Numerical Verification of the Plane

The full development process of different Pr fluids in a constant heat flow heated plane was studied using DNS (Kawamura et al., 1998; Kawamura et al., 1999; Tiselj and Cizelj, 2012). This study compares the DNS data with $Pr = 0.01 \sim 0.05$. The plane geometry and mesh parameters are

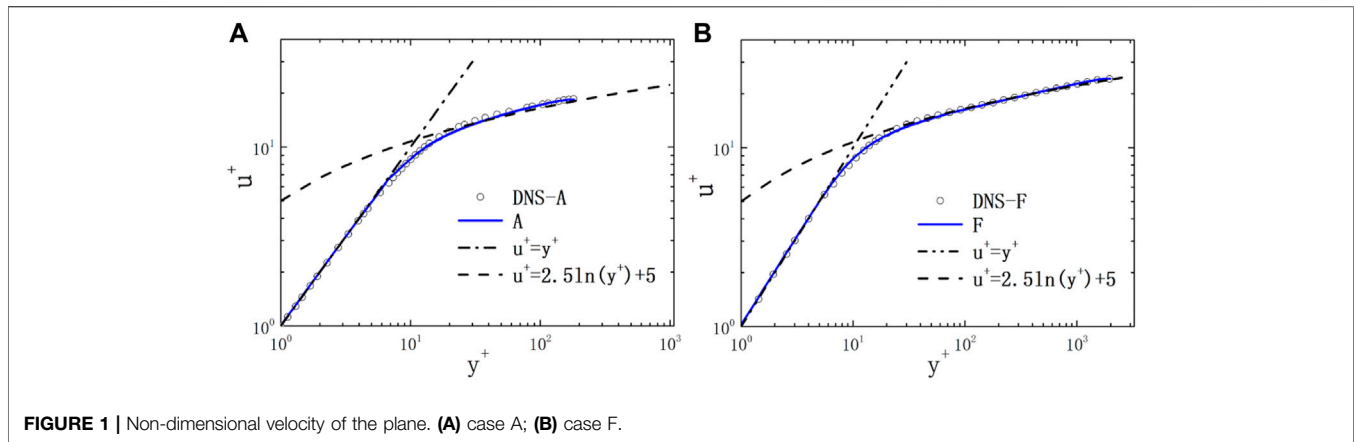


FIGURE 1 | Non-dimensional velocity of the plane. (A) case A; (B) case F.

consistent with those in the literature (Su et al., 2021; Su and Gu, 2021). Here, the three-dimensional parallel plane with a flow length of 6.4 h, a spanwise width of 3.2 h, and a plane height of 2 h were selected as the calculation domain, where h is the half-height of the plane, 30.25 mm. The wall heat flux is set as $q_w = 360 \text{ kW/m}^2$. Finally, 80, 50, and 100 nodes are divided into three directions, respectively: Flow direction, span direction, and height. Due to the symmetry of the plane, half of the plane is taken as the calculation domain, and the structured grid is used. The grid height of the first boundary layer is set to $3 \times 10^{-6} \text{ m}$ to meet the requirements of the low Reynolds number turbulence model, $y^+ < 1$. The physical properties of $Pr = 0.01\text{--}0.05$ are reported in **Table 3**. The friction Reynolds number $Re_\tau = u_\tau h/\nu$ is taken as the calculation conditions: 180 (A), 395 (B), 590 (C), 640 (D), 950 (E), 2000 (F), and 4,400 (G), where u_τ is the friction velocity on the wall side, h is the half-height of the plane, and the numbers A ~ G represent different Reynolds number calculation conditions. For the convenience of analysis, u_τ and the friction temperature T_τ are taken as the dimensionless reference quantity, where T_τ is set as $q_w \rho^{-1} C_p^{-1} u_\tau^{-1}$, and q_w is the wall heat flux.

3.2.1 Velocity Field Verification

The dimensionless velocity $u^+ = u/u_\tau$ distribution of cases A and F along the dimensionless wall-normal distance $y^+ = yu_\tau/\nu$ is shown in **Figure 1**. At a low Reynolds number and a high Reynolds number, the velocity distribution predicted by the present isotropic four-equation model is in good agreement with the DNS results, and the velocity distribution meets $u^+ = y^+$ in the linear region ($u^+ = y^+$) while it meets $u^+ = 2.51 \ln y^+ + 5$ in the logarithmic rate region ($y^+ > 30$).

The distribution of dimensionless Reynolds stress $\tau_R^+ = \overline{u'v'}/u_\tau^2$ and total shear stress $\tau_{total}^+ = \tau_R^+ + \nu u_{,y} u_\tau^{-2}$ along y^+ under cases A and F is shown in **Figure 2**. The stress calculation results are in good agreement with DNS results. In the near-wall region ($1 < y^+ < 7$), this study predicted τ_R^+ to be lower than the DNS value. However, it has little effect on the calculation results of the velocity field in the linear region, mainly because the molecular diffusion is dominant in the near-wall region. With the increase in wall distance, the turbulent diffusion effect

increases gradually. When $y^+ > 30$, the total shear stress coincides with the Reynolds stress curve.

3.2.2 Temperature Field Verification

1) $Pr = 0.01$

The dimensionless temperature $\theta^+ = \theta/T_\tau$ distribution of the $Pr = 0.01$ fluid along y^+ is shown in **Figure 3A**. Cases A, B, and C agree with DNS and meet $\theta^+ = Pr y^+$ in the linear region ($1 < y^+ < 40$).

The distribution of dimensionless Reynolds heat flux $q_R^+ = -\alpha_t \theta_{,y} u_\tau^{-1} T_\tau^{-1}$ and total heat flux $q_{total}^+ = -(\alpha_t + \alpha) \theta_{,y} u_\tau^{-1} T_\tau^{-1}$ along y^+ is shown in **Figures 3B–D**. The heat flux calculation results of cases A–C are in good agreement with DNS results. Due to the thick thermal boundary layer and strong molecular heat conduction of low Pr fluid, although the predicted Reynolds heat flux deviates from the DNS results at $1 < y^+ < 30$, it does not affect the linear distribution of the temperature field in this region. With the increase in wall distance, although the effect of turbulent heat diffusion is gradually increasing, there is still a difference between the total heat flow and Reynolds heat flux, mainly caused by the strong molecular heat conduction of low Pr fluid.

2) $Pr = 0.025$

The distribution of θ^+/Pr of the $Pr = 0.025$ fluid along y^+ is shown in **Figure 4A**. Cases A, B, and C are in good agreement with DNS. The peak value of θ^+/Pr increases with the increase in the Reynolds number. The distribution of q_R^+ along y^+ is shown in **Figure 4B**. Cases A and B agree with DNS. With the increase in Re , the q_R^+ peak increases and moves to the turbulent core.

3) $Pr = 0.05$

As shown in **Figure 5A**, the dimensionless temperature θ^+ of case A of $Pr = 0.05$ fluid is in good agreement with the DNS results. At the same Reynolds number, with the decrease in Pr , the molecular thermal conductivity increases and the average θ^+ decreases. As shown in **Figure 5B**, the dimensionless Reynolds

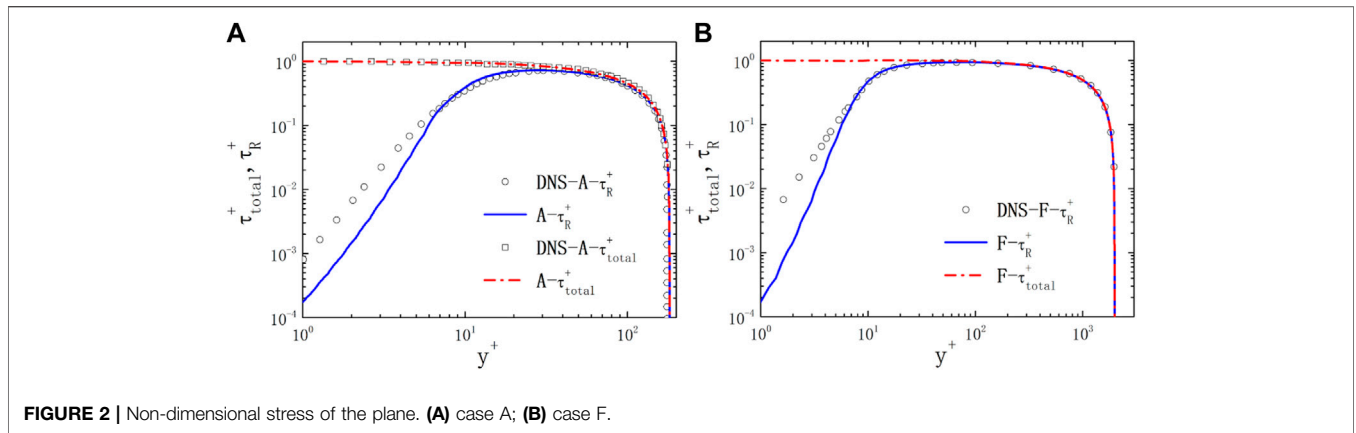


FIGURE 2 | Non-dimensional stress of the plane. **(A)** case A; **(B)** case F.

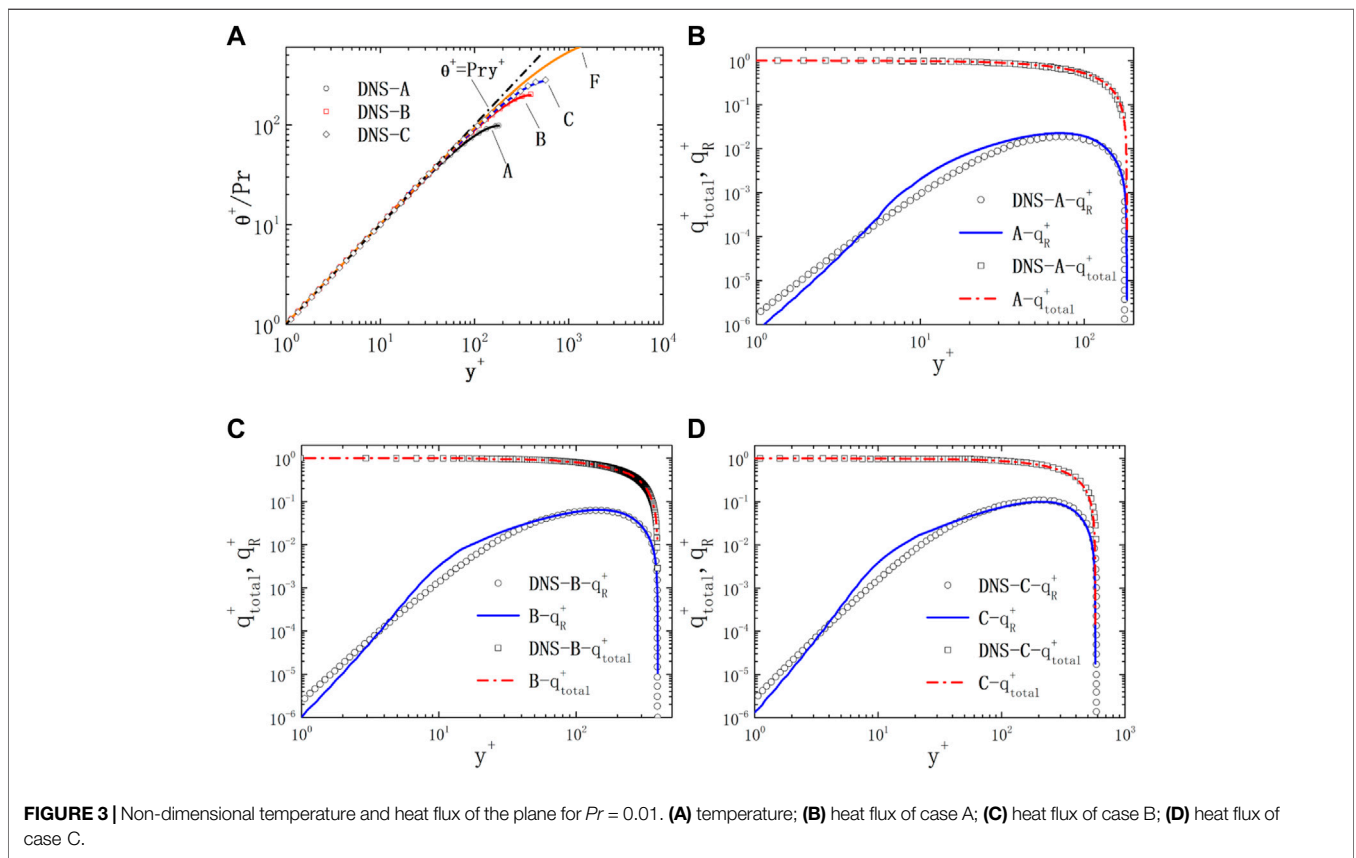


FIGURE 3 | Non-dimensional temperature and heat flux of the plane for $Pr = 0.01$. **(A)** temperature; **(B)** heat flux of case A; **(C)** heat flux of case B; **(D)** heat flux of case C.

heat flux of case A of $Pr = 0.05$ fluid is in good agreement with the DNS results.

3.3 Numerical Analysis of the Square Bundle

To further analyze the applicability of the current isotropic four-equation model in complex geometries, the flow and heat of liquid metal with a Prandtl value of 0.01 in the quadrilateral infinite rod bundle were studied. **Figure 6** shows the schematic diagram of the computational domain and local hexahedral mesh of the quadrilateral infinite rod bundle. Lines ab, bo, oc, and arc ca are the local distributions to be analyzed next. The flow

parameters are reported in **Table 4**. The surfaces of rods in contact with the fluids are heated by uniform wall fluxes q_w . Symmetry condition is applied on other faces to simulate the infinite rod bundle region with a quadrilateral arrangement. The heat fully developed flow length L_z is set to $10D_h$ (Ge et al., 2017). The rod diameter D and $X = P/D$ ratio are the same as in Zhukov’s experiment (Zhukov et al., 2002).

3.3.1 Heat Transfer Evaluation and Analysis

In **Table 5**, a few important heat transfer correlations of Nusselt number Nu are available for the quadrilateral infinite rod bundle,

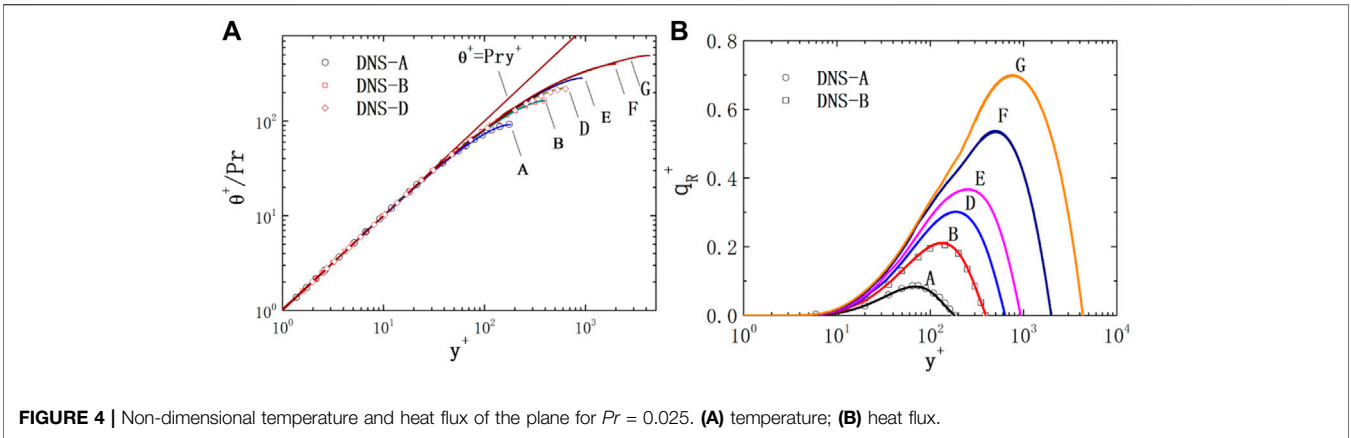


FIGURE 4 | Non-dimensional temperature and heat flux of the plane for $Pr = 0.025$. (A) temperature; (B) heat flux.

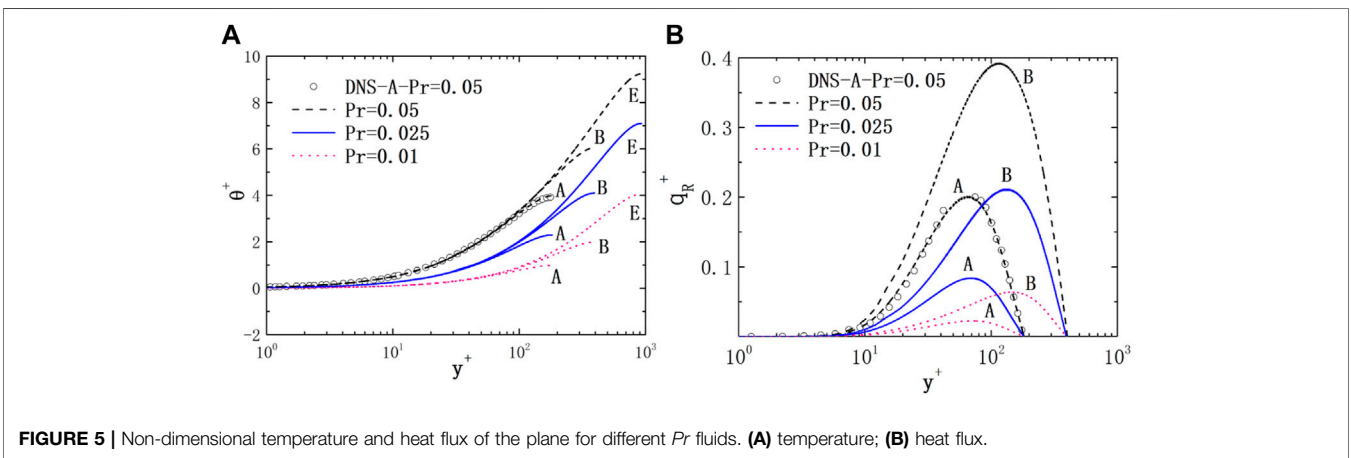


FIGURE 5 | Non-dimensional temperature and heat flux of the plane for different Pr fluids. (A) temperature; (B) heat flux.

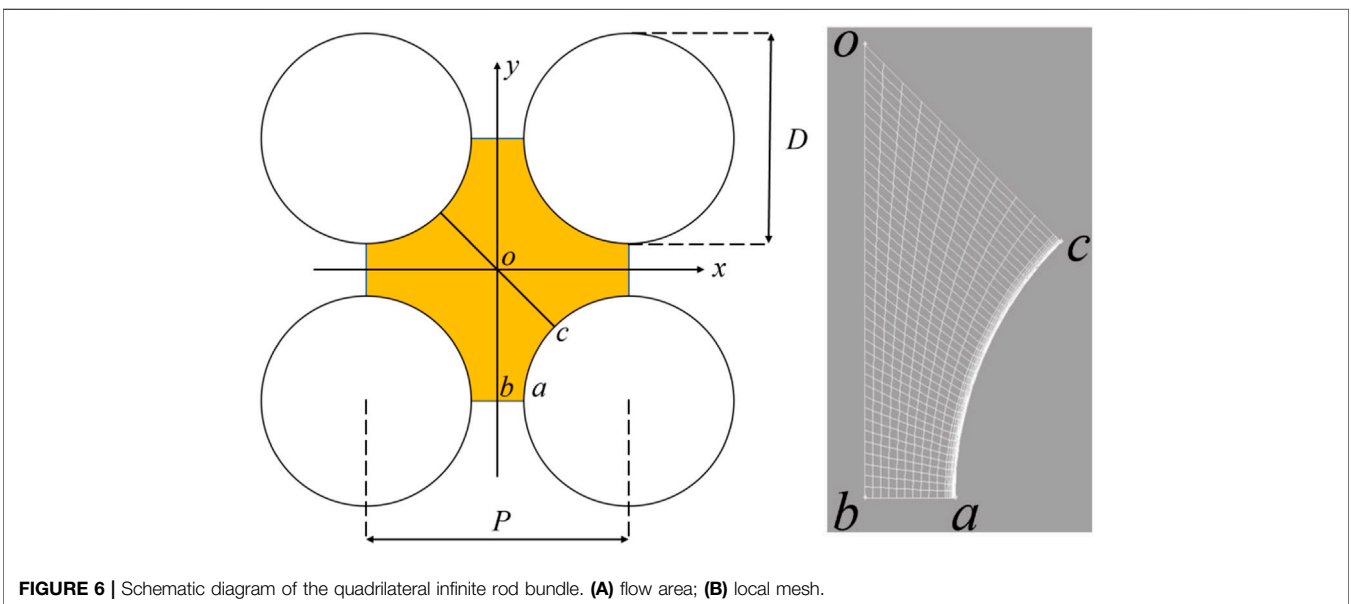


FIGURE 6 | Schematic diagram of the quadrilateral infinite rod bundle. (A) flow area; (B) local mesh.

TABLE 4 | Flow parameters.

Parameter	Symbol	Value	Unit
Prandtl numbers	Pr	0.01	—
Rod diameter	D	12	mm
P/D ratios	X	1.25, 1.34, 1.46	—
Peclet numbers	Pe	250–4,000	—
Reynolds numbers	Re	25,000–400,000	—

reviewed in the study by (Mikityuk 2009). Zhukov (Zhukov et al., 2002) obtained 36 $Nu(Pe)$ data from the heat transfer experiment of 22%Na–78%K in a quadrilateral rod bundle. The correlations obtained by Subbotin (Subbotin et al., 1965) and BREST (Adamov 2001) were derived from triangular bundles, while Mikityuk, from a wide database, conducted experimental results of liquid metals (Mikityuk 2009). It is worth noting that there are no more available experimental data. The

correlations should be used with care and be paid more attention to for analysis of the reliability. The Nu can be calculated as follows:

$$Nu = \frac{q_w D_h}{\lambda(T_{wm} - T_b)}, T_b = \frac{\int_A u_i n_i T dA}{\int_A u_i n_i dA}, T_{wm} = \frac{\int_{\Gamma_w} T ds}{\int_{\Gamma_w} ds} \quad (32)$$

where n_i is a vector of a unit perpendicular to a sliced face.

First, the simulations for $Pr = 0.01$ are characterized by $X = 1.25, 1.34,$ and 1.46 with a corresponding hydraulic diameter D_h of 11.87, 15.43, and 20.57 mm. Nine simulations with bulk Reynolds numbers of 250–400,000 were operated. The corresponding Peclet number is approximately 250–4,000. **Figure 7** shows the Nusselt number results for $X = 1.25 - 1.46$ cases. In **Figure 7**, Subbotin and Mikityuk correlations overestimated the Nusselt number compared with the conservative result of Zhukov and BREST. The correlation

TABLE 5 | Correlations of Nusselt number for the square bundle.

Investigator	Correlation	X	Pe
Zhukov et al.	$Nu = 7.55X - 14X^{-5} + 0.007Pe^{0.64+0.246X}$	1.25–1.46	60–2000
Subbotin et al.	$Nu = 0.58(\frac{4}{\pi}X^2 - 1)^{0.55}Pe^{0.45}$	1.1–1.5	80–4,000
BREST	$Nu = 7.55X - 20X^{-5} + \frac{0.0354}{X^2}Pe^{0.56+0.204X}$	1.28–1.46	100–1,600
Mikityuk	$Nu = 0.047(1 - \exp^{-3.8(X-1)})(Pe^{0.77} + 250)$	1.1–1.95	30–5,000

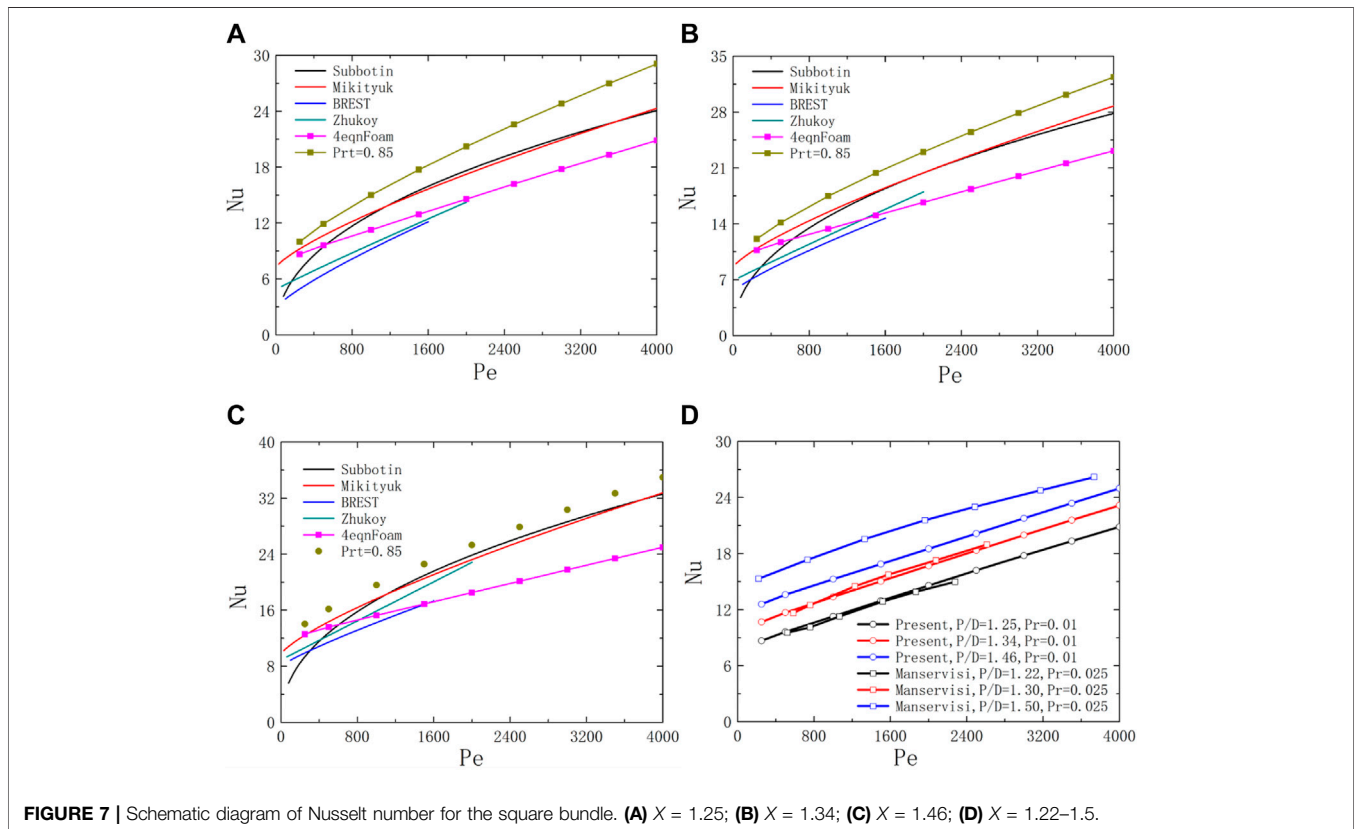


FIGURE 7 | Schematic diagram of Nusselt number for the square bundle. (A) $X = 1.25$; (B) $X = 1.34$; (C) $X = 1.46$; (D) $X = 1.22-1.5$.

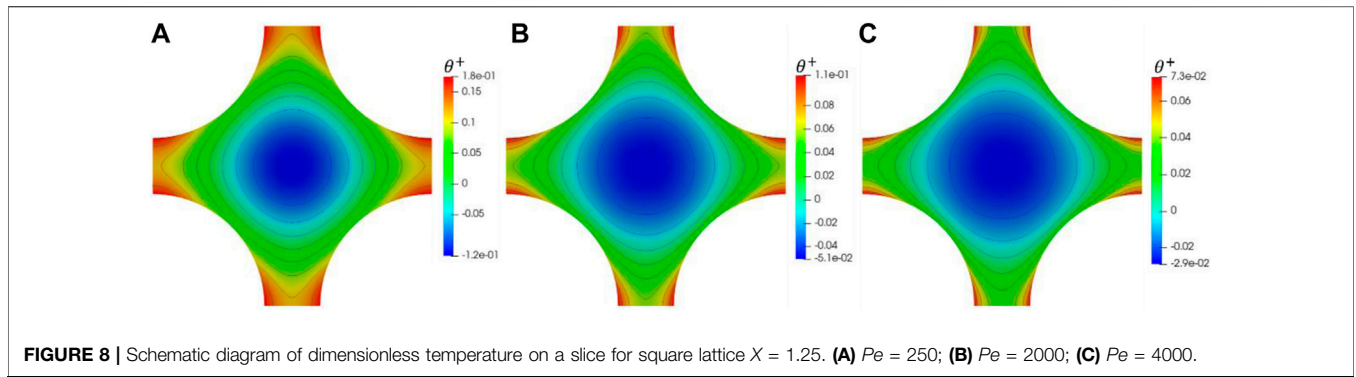


FIGURE 8 | Schematic diagram of dimensionless temperature on a slice for square lattice $X = 1.25$. **(A)** $Pe = 250$; **(B)** $Pe = 2000$; **(C)** $Pe = 4000$.

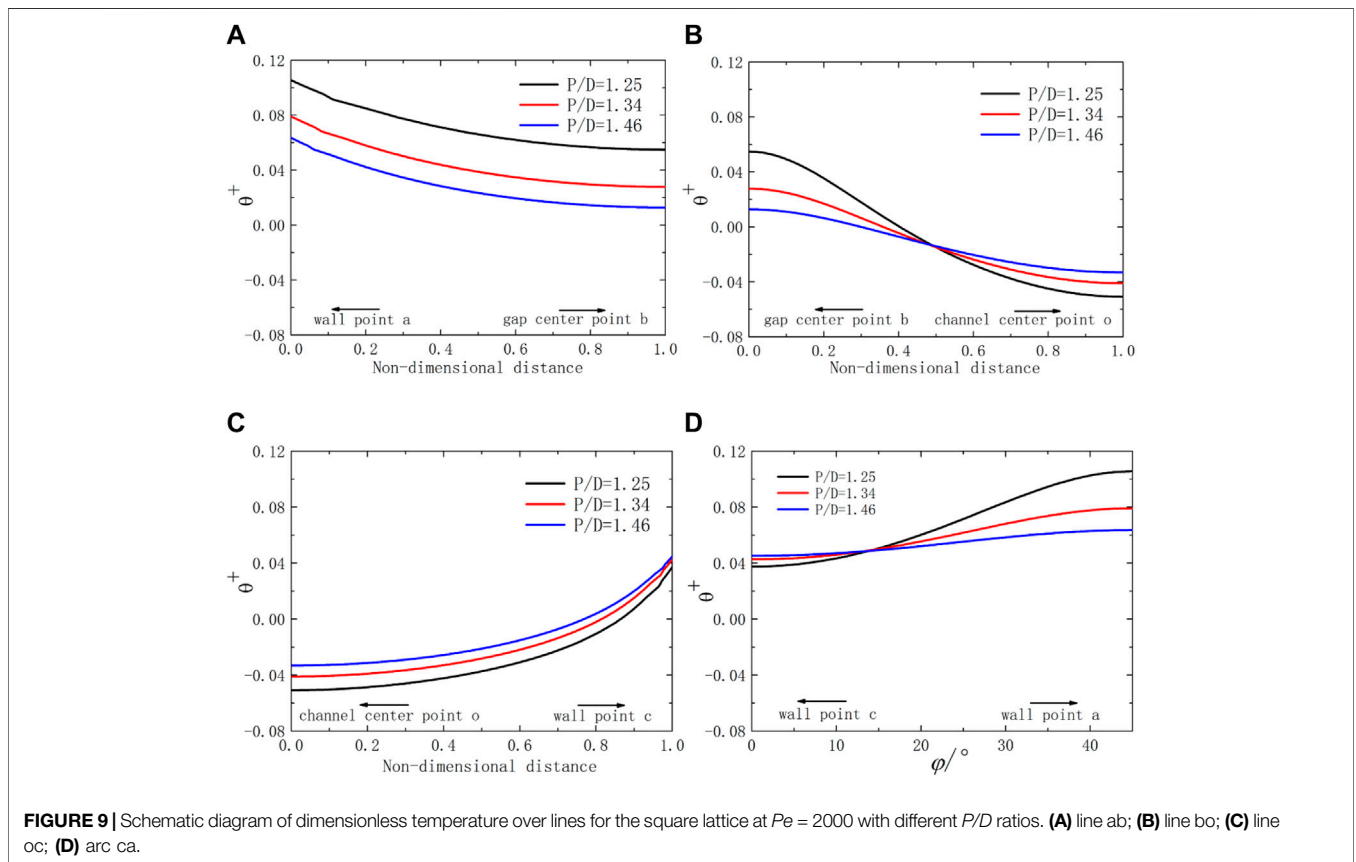


FIGURE 9 | Schematic diagram of dimensionless temperature over lines for the square lattice at $Pe = 2000$ with different P/D ratios. **(A)** line ab; **(B)** line bo; **(C)** line oc; **(D)** arc ca.

between these empirical relations is too poor to relate because these relationships have very different slopes.

In **Figures 7A–C**, the prediction Nu of the isotropic $k - \tilde{\epsilon} - k_\theta - \tilde{\epsilon}_\theta$ model almost lies between the experimental relationship. The prediction of the $Pr_t = 0.85$ model is higher than Subbotin and Mikityuk correlations. At low Peclet numbers, the Nu results having a special slope predicted using the isotropic four-equation model is closer to the Subbotin and Mikityuk correlations, while the calculation results at high Pe are conservative, similar to the Zhukov and BREST correlations. The overall numerical Nu seems to be more conservative than these experimental correlations. Poor experimental relevance makes this problem’s numerical verification difficult to go on.

As shown in **Figure 7D**, the numerical slope in the $Nu(Pe)$ line obtained using the $k - \tilde{\epsilon} - k_\theta - \tilde{\epsilon}_\theta$ model is very similar to that predicted using Manservigi’s $k - \epsilon - k_\theta - \epsilon_\theta$ model, which has successfully predicted heat transfer calculation for $Pr = 0.025$ fluids and can provide an additional CFD relationship reference. Therefore, we still use the present isotropic four-equation model for thermal analysis and local temperature calculations.

This present work focuses on the comparison of the effects of two turbulent thermal diffusion models (the $Pr_t = 0.85$ model and the present isotropic $k - \tilde{\epsilon} - k_\theta - \tilde{\epsilon}_\theta$ model) on the temperature field, without considering the influence of different RANS turbulence $k - \epsilon$ or $k - w$ models. The detailed

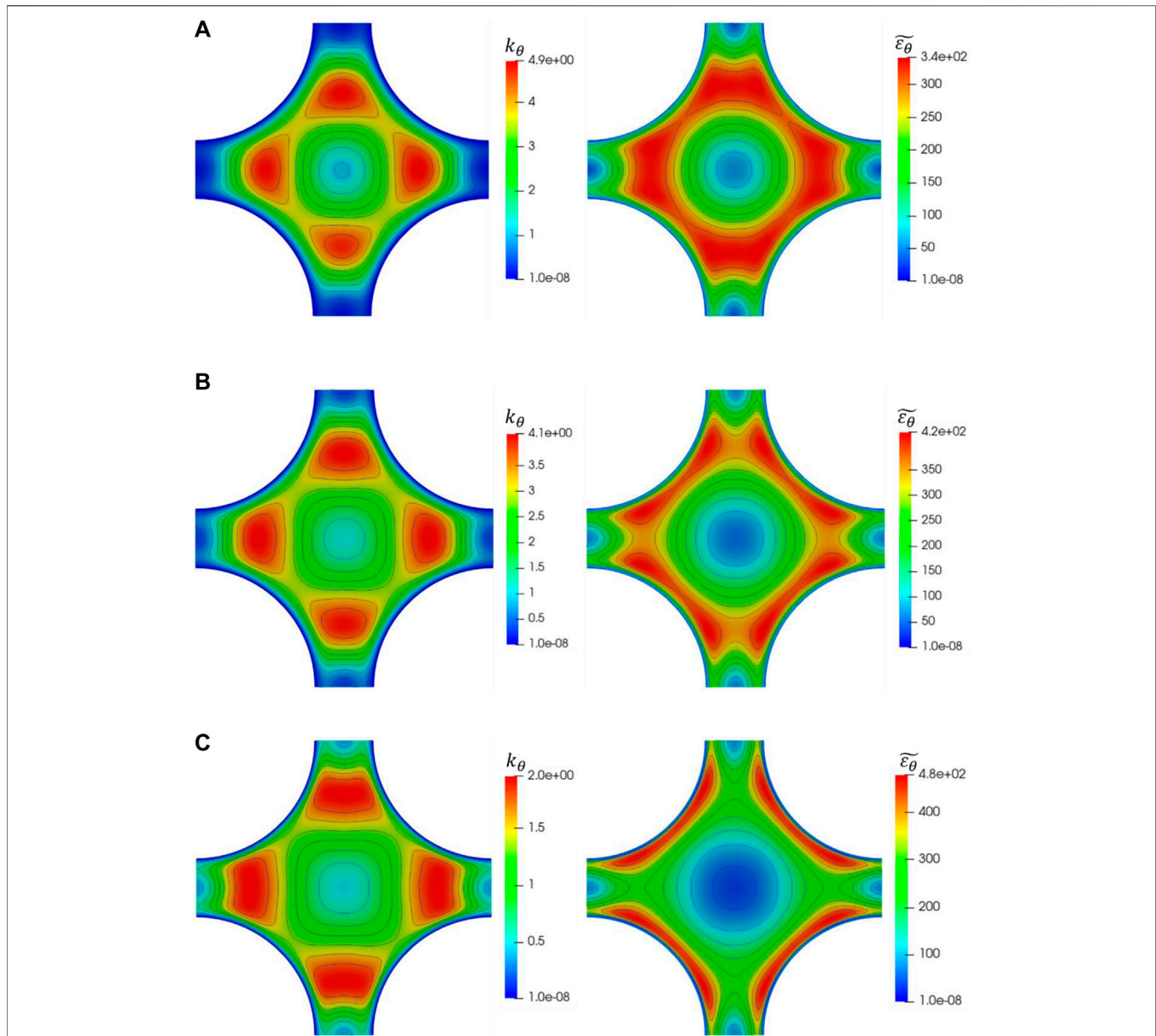


FIGURE 10 | Schematic diagram of average temperature fluctuation (left) and its isotropic dissipation (right) on a slice for square lattice $X = 1.25$. **(A)** $Pe = 1000$; **(B)** $Pe = 2000$; **(C)** $Pe = 4000$.

influence and performance evaluation of different turbulence models on liquid metal flow can be found in the literature (You et al., 2019).

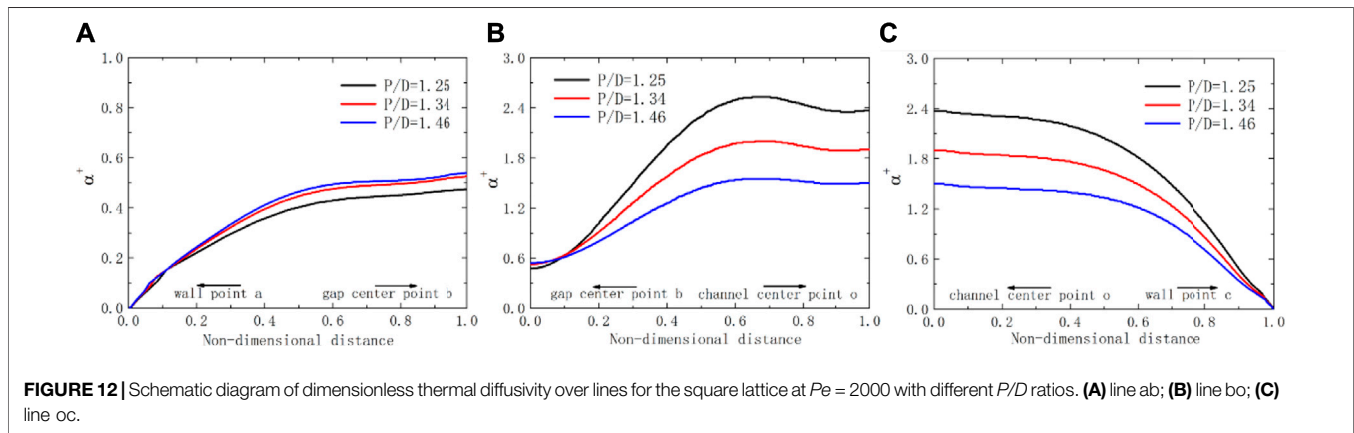
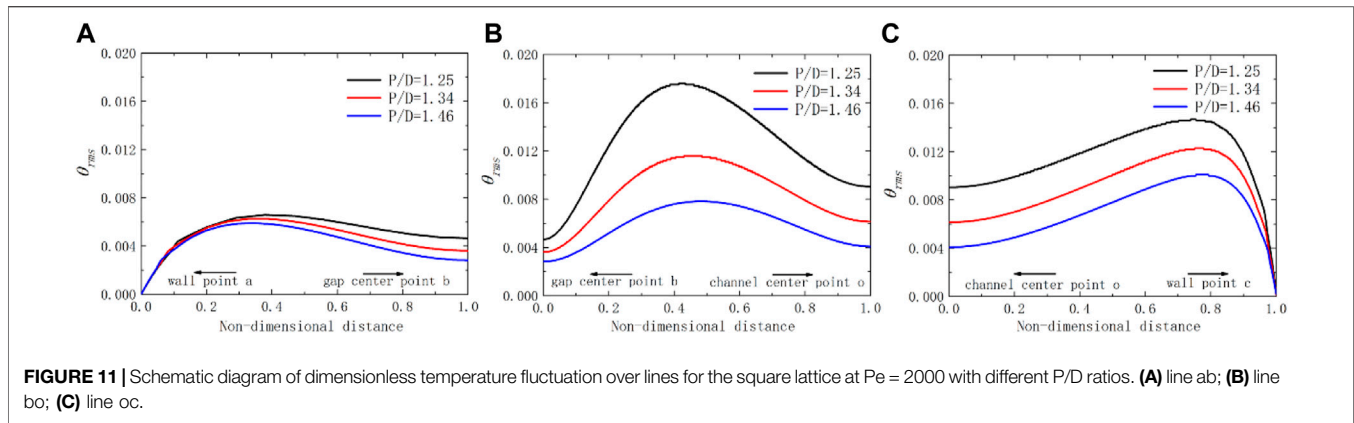
3.3.2 Turbulent Thermal Fields

1) Coolant and wall temperature

Figure 8 shows the dimensionless temperature $\theta^+ = \lambda(T - T_b)/(q_w \cdot D_h)$ on a sliced surface of square bundle $X = 1.25$. The overall dimensionless temperature in the channel decreases with the increase in Pe . The temperature at the rod surface is not constant. The wall temperature near

the center of the channels is lower than that near the center of gaps.

Figure 6 has annotated the line ab, line bo, line oc, and arc ca, where points b and c represent the center of the gap and the channel, respectively. The dimensionless temperature field with $Pe = 2000$ is selected for analysis. In **Figure 9A**, with the decrease in P/D , the gap width decreases, and the overall dimensionless temperature distribution θ^+ at the gap line ab increases. In **Figures 9B,D**, the coolant dimensionless temperature distribution from gap center point b to channel center point o and the wall dimensionless temperature distribution over arc ca are smoother in pace with strengthening of P/D . Due to the



development of velocity and sufficient cooling of the fluid near the center of the channel, the dimensionless temperature distribution over line oc decreases when the value of P/D decreases in **Figure 9C**.

2) Fluctuation and isotropic dissipation

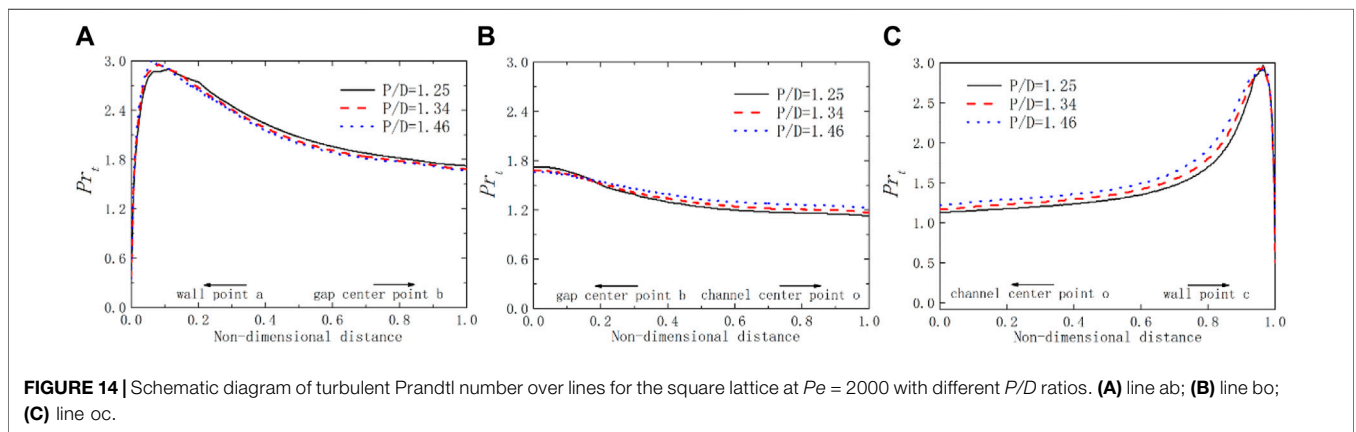
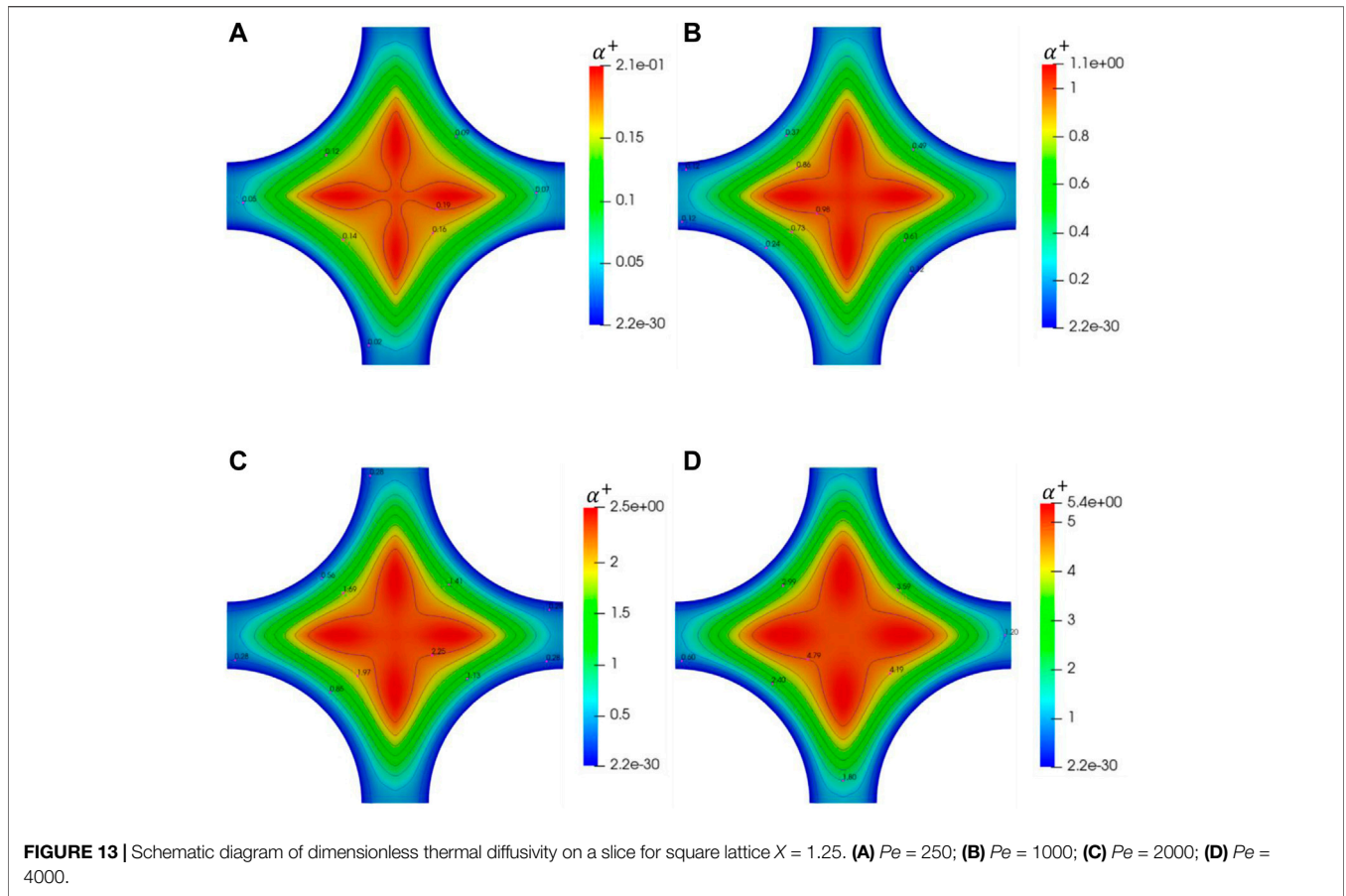
The distribution and shape of k_θ and $\tilde{\varepsilon}_\theta$ for $Pe = 100, 2000$, and $4,000$ are shown in **Figure 10**. k_θ has a lower local value near the center point o. The maximum value appears near the wall. The maximum value of k_θ decreases when Pe increases, while that of ε_θ increases. The numerical shape and distribution of k_θ and its isotropic dissipation $\tilde{\varepsilon}_\theta$ obtained from the present $k - \tilde{\varepsilon} - k_\theta - \tilde{\varepsilon}_\theta$ model is similar to that predicted by Manservigi's $k - \varepsilon - k_\theta - \varepsilon_\theta$ model (Manservigi and Menghini, 2015). Further details on over line ab, line bo, and line oc can be found in **Figure 11**. The dimensionless root square means temperature $\theta_{rms} = \lambda\sqrt{2k_\theta}/(qD_h)$ is set. From wall point a to wall point b, θ_{rms} first increases to a small peak and then begins to decrease to point b. Then along the bo line, the maximum peak value of θ_{rms} is reached near the midpoint of the bo section. Three peaks of different sizes were formed on lines ab, bo, and oc, respectively. When it goes straight toward the wall point, it will eventually approach 0. When the value is X , the overall value of θ_{rms} decreases.

3) Turbulence and molecular thermal diffusivity

Figure 12 shows the proportional relationship of turbulent to molecular thermal diffusivity, that is, dimensionless thermal diffusivity $a^+ = \alpha_t/\alpha$, over line ab, line bo, and line oc with the change of P/D for square bundle $X = 1.25$ at $Pe = 2000$. Reynolds heat flux q_t and molecular heat flux q_m can be defined as follows:

$$q_t = -\overline{v'\theta'} = \alpha_t \frac{\partial T}{\partial y}, q_m = \alpha_m \frac{\partial T}{\partial y} \quad (33)$$

Thus, the specific value of turbulent to molecular thermal diffusivity represents the ratio of Reynolds to molecular heat flux. Reynolds heat flux is mainly caused by thermal diffusion caused by turbulent flow, while molecular heat conduction generates molecular heat flux. In **Figure 12**, in the area closest to the wall point a or c, a^+ tends to 0, which means turbulent heat diffusion tends to be ignored here. With the increase in wall distance from wall point a to gap center point b, the turbulent heat diffusion gradually increases, so the value of a^+ increases. However, a^+ is still less than one over line ab, which means that the molecular heat conduction of liquid metal always affects the heat transfer at the gap area. At the gap center point b, a^+ reaches a local maximum over



line ab. It increases along the bo segment and reaches its maximum near the middle of the bo segment. In most regions far from the wall over lines bo and oc, due to the development of the turbulent flow, turbulent diffusion is greater than the molecular heat conduction, so $a^+ > 1$. Interestingly, the maximum value of a^+ does not appear at the channel center point o but near point o. At the gap line ab, the smaller the gap length, the greater the influence of molecular heat conduction, so the value of a^+ increases

over the line ab when the value of P/D increases. But it decreases over the line bo and line oc when the value of P/D increases because at the same Pe , the larger the P/D , the larger the flow area, the smaller the overall velocity, and the smaller the turbulent heat diffusion over those areas. In **Figure 13**, the dimensionless thermal diffusivity on a slice for $Pe = 250, 1,000, 2,000$, and $4,000$ is shown. At the same P/D , when the Pe increases, turbulent heat diffusion will be enhanced, and the grid point with $a^+ > 1$ begins to appear.

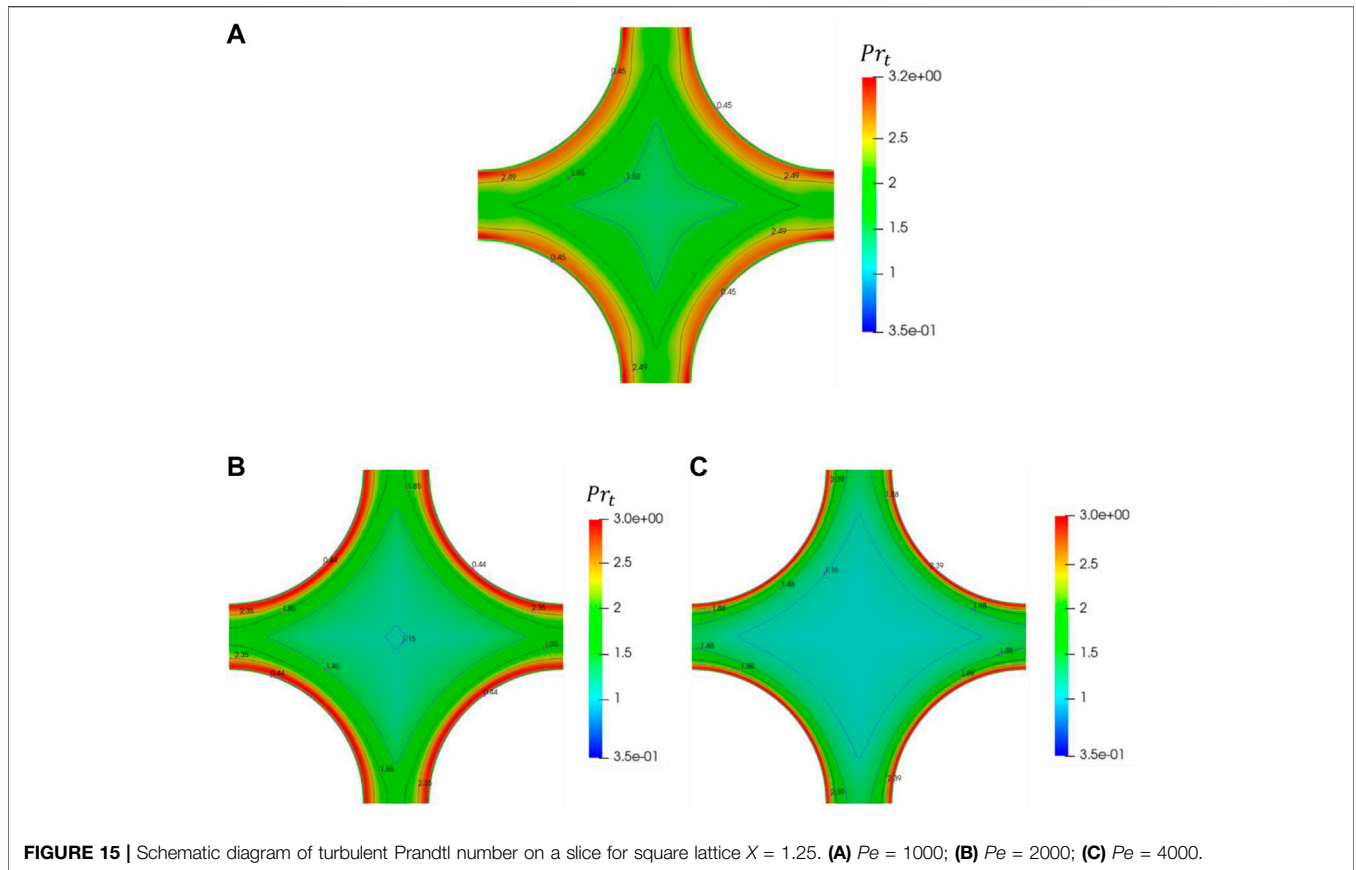


TABLE 6 | Average turbulent Prandtl number under different P/D and Pe .

Pe/X	1.25	1.34	1.46
250	2.82087	2.98207	3.157
500	2.4074	2.46975	2.55527
1,000	2.05343	2.10667	2.16182
1,500	1.85231	1.89726	1.94714
2000	1.71413	1.75079	1.79239
2,500	1.60956	1.64109	1.67649
3,000	1.52892	1.55685	1.58799
3,500	1.46592	1.49062	1.51881
4,000	1.41584	1.43757	1.46309

The average turbulent Prandtl number Pr_{tm} can be defined as follows:

$$Pr_{tm} = \frac{\int_A Pr_t dA}{\int_A dA} \quad (34)$$

Table 6 summarizes the calculation results of average turbulent Prandtl number Pr_{tm} under different P/D and Pe using the present $k - \tilde{\epsilon} - k_\theta - \tilde{\epsilon}_\theta$ model. One can see that at the same P/D , the average turbulent Prandtl number decreases with the increase in Pe , while at the same Pe , it increases when the value of P/D increases.

4) Turbulent Prandtl number

In **Figure 14**, the Pr_t with the change of P/D is shown over the lines ab, bo, and oc for the square bundle with $X = 1.25$ at $Pe = 2000$. The Pr_t is not constant and linear. It is larger than the general value of 0.85 for liquid metal. The Pr_t distribution on the line bo is to be smoother than that of lines ab and co. The value of Pr_t decreases over line ab when the value of P/D increases, while it increases over lines bo and oc. This phenomenon echoes the changing trend of dimensionless thermal diffusivity. In **Figure 15**, the turbulent Prandtl number on a slice for $Pe = 1,000, 2000$, and $4,000$ for the square bundle is shown. When Pe increases, Pr_t near the wall and the center decreases gradually.

5) Performance analysis of the present four-equation model

When the same turbulence $k - \tilde{\epsilon}$ model is kept to solve the turbulent viscosity, the present four-equation model needs to solve two more equations $k_\theta - \tilde{\epsilon}_\theta$ than the $Pr_t = 0.85$ model. To analyze the calculation speed of the $k - \tilde{\epsilon} - k_\theta - \tilde{\epsilon}_\theta$ model, the single-step iterative calculation time and calculation memory of these two models are compared and listed in **Table 7**. The current test platform is HP ProDesk 680 G4 MT with an Intel(R) Core(TM) i7-9700 CPU at 3.00 GHz and 16 GB system memory at 2,667 MHz. At present, the model solver is written based on OpenFOAM V6 version, compiled and integrated in Ubuntu 18.04 system environment. As shown in **Table 7**, the calculation time and memory required by the

TABLE 7 | Performance of the four-equation model under serial operation.

X	Pe	Models	Meshes/million	Single-step iteration duration/s	Memory usage/MB
1.25	1,000	$k - \tilde{\varepsilon} - k_{\theta} - \tilde{\varepsilon}_{\theta}$	1.40	10.19	2,459
		$k - \tilde{\varepsilon} - Pr_t = 0.85$		7.31	2,107
1.34	1,000	$k - \tilde{\varepsilon} - k_{\theta} - \tilde{\varepsilon}_{\theta}$	2.46	21.83	3,766
		$k - \tilde{\varepsilon} - Pr_t = 0.85$		17.42	3,458
1.46	1,000	$k - \tilde{\varepsilon} - k_{\theta} - \tilde{\varepsilon}_{\theta}$	4.24	43.56	5,500
		$k - \tilde{\varepsilon} - Pr_t = 0.85$		37.68	5,311

$k - \tilde{\varepsilon} - k_{\theta} - \tilde{\varepsilon}_{\theta}$ model are greater than those of the $k - \tilde{\varepsilon} - Pr_t = 0.85$ model.

4 CONCLUSION

The present work studied an isotropic four-equation model for low Pr number that uses simple Dirichlet wall boundaries. First, the turbulent heat transfer process of $Pr = 0.01 \sim 0.05$ fluid in the uniformly heated plane is numerically studied on the open-source program OpenFOAM. Then the flow and heat of the isotropic four-equation of the quadrilateral infinite rod bundle region are evaluated and analyzed with low Prandtl number $Pr = 0.01$. In the SGDH framework, the $Pr_t = 0.85$ model and the isotropic four-equation model are compared with available experimental correlations in the range of $Pe = 250\text{--}4,000$ and $P/D = 1.25\text{--}1.46$. The numerical results show that.

- 1) The full development velocity, temperature, Reynolds stress, and Reynolds heat flow of $Pr = 0.01 \sim 0.05$ fluid in-plane predicted using the isotropic four-equation model are in good agreement with the DNS results.
- 2) The Nu of the isotropic four-equation model lies between the experimental relationship, more conservative and similar to the Zhukov and BREST correlations for square rod bundles, while the $Pr_t = 0.85$ model gives too high a Nusselt number prediction to predict the integra heat properly. The slope of Nu predicted by the present isotropic four-equation model is similar to Manservisi's model.
- 3) More detailed heat exchange phenomena and local temperature distribution are obtained using the four-equation model. At the same P/D , the average turbulent

Prandtl number decreases with the increase in Pe, while at the same Pe, it increases when the value of P/D increases.

The isotropic four-equation model can provide more references for calculating the thermal-hydraulic phenomena of liquid metals. But its wider applicability needs further verification.

DATA AVAILABILITY STATEMENT

The raw data supporting the conclusion of this article will be made available by the authors, without undue reservation.

AUTHOR CONTRIBUTIONS

XS: concept, research, writing, editing, code, and data processing. XL: modification, concept, research, and code. XW: research, modification, and code. YL: concept, editing, and research. QC: editing and research. QS: editing and research. XS: editing and research. GL: funding, project management, concept, and research.

FUNDING

This work was supported by the Research on key technology and safety verification of primary circuit, Grant No. 2020YFB1902104, and the Experimental study on thermal-hydraulics of fuel rod bundle, Grant No. Y828020XZ0.

REFERENCES

- Abe, K., Kondoh, T., and Nagano, Y. (1995). A New Turbulence Model for Predicting Fluid Flow and Heat Transfer in Separating and Reattaching Flows-II. Thermal Field Calculations. *Int. J. Heat Mass Transfer* 38 (8), 1467–1481. doi:10.1016/0017-9310(94)00252-q
- Adamov, E. O. (2001). *Naturally Safe Lead-Cooled Fast Reactor for LargeScale Nuclear Power*. Moscow: Dollezhal RDIPE.
- Cerroni, D., Da Vià, R., Manservisi, S., Menghini, F., Pozzetti, G., and Scardovelli, R. (2015). Numerical Validation of $k - \omega - K\theta - \Omega\theta$ heat Transfer Turbulence Model for Heavy Liquid Metals. *J. Phys. Conf. Ser.* 655 (1), 012046. doi:10.1088/1742-6596/655/1/012046
- Cheng, X., and Tak, N.-i. (2006). Investigation on Turbulent Heat Transfer to lead-bismuth Eutectic Flows in Circular Tubes for Nuclear Applications. *Nucl. Eng. Des.* 236 (4), 385–393. doi:10.1016/j.nucengdes.2005.09.006
- Chierici, A., Chirco, L., Da Vià, R., and Manservisi, S. (2019). Numerical Simulation of a Turbulent Lead Bismuth Eutectic Flow inside a 19 Pin Nuclear Reactor Bundle with a Four Logarithmic Parameter Turbulence Model. *J. Phys. Conf. Ser.* 1224, 012030. doi:10.1088/1742-6596/1224/1/012030
- Choi, S. K., and Kim, S. O. (2007). Treatment of Turbulent Heat Fluxes with the Elliptic-Blending Second-Moment Closure for Turbulent Natural Convection Flows. *Int. J. Heat Mass Transfer* 51 (9-10), 2377–2388. doi:10.1016/j.ijheatmasstransfer.2007.08.012
- Da Vià, R., Giovacchini, V., and Manservisi, S. (2020). A Logarithmic Turbulent Heat Transfer Model in Applications with Liquid Metals for $Pr = 0.01\text{--}0.025$. *Appl. Sci.* 10 (12), 4337. doi:10.3390/app10124337
- Da Vià, R., and Manservisi, S. (2019). Numerical Simulation of Forced and Mixed Convection Turbulent Liquid Sodium Flow over a Vertical Backward Facing Step with a Four Parameter Turbulence Model. *Int. J. Heat Mass Transfer* 135, 591–603. doi:10.1016/j.ijheatmasstransfer.2019.01.129

- Da Vià, R., Manservigi, S., and Menghini, F. (2016). A $K-\Omega-K\theta-\Omega\theta$ Four Parameter Logarithmic Turbulence Model for Liquid Metals. *Int. J. Heat Mass Transfer* 101 (10), 1030–1041. doi:10.1016/j.jheatmasstransfer.2016.05.084
- Deng, B., Wu, W., and Xi, S. (2001). A Near-wall Two-Equation Heat Transfer Model for wall Turbulent Flows. *Int. J. Heat Mass Transfer* 44 (4), 691–698. doi:10.1016/s0017-9310(00)00131-9
- Duponcheel, M., Bricteux, L., Manconi, M., Winkelmans, G., and Bartosiewicz, Y. (2014). Assessment of RANS and Improved Near-wall Modeling for Forced Convection at Low Prandtl Numbers Based on LES up to $Re\tau=2000$. *Int. J. Heat Mass Transfer* 75, 470–482. doi:10.1016/j.jheatmasstransfer.2014.03.080
- Ejzenstam, J., and Szakálos, P. (2015). Long Term Corrosion Resistance of Alumina Forming Austenitic Stainless Steels in Liquid lead. *J. Nucl. Mater.* 461, 164–170. doi:10.1016/j.jnucmat.2015.03.011
- Ge, Z., Liu, J., Zhao, P., Nie, X., and Ye, M. (2017). Investigation on the Applicability of Turbulent-Prandtl-Number Models in Bare Rod Bundles for Heavy Liquid Metals. *Nucl. Eng. Des.* 314, 198–206. doi:10.1016/j.nucengdes.2017.01.032
- Groetzbach, G. (2013). Challenges in Low-Prandtl Number Heat Transfer Simulation and Modelling. *Nucl. Eng. Des.* 264, 41–55. doi:10.1016/j.nucengdes.2012.09.039
- Gu, L., and Su, X. (2021). Latest Research Progress for LBE Coolant Reactor of China Initiative Accelerator Driven System Project. *Front. Energ.* 15, 810–831. doi:10.1007/s11708-021-0760-1
- Kawamura, H., Abe, H., and Matsuo, Y. (1999). DNS of Turbulent Heat Transfer in Channel Flow with Respect to Reynolds and Prandtl Number Effects. *Int. J. Heat Fluid Flow* 20 (3), 196–207. doi:10.1016/s0142-727x(99)00014-4
- Kawamura, H., Ohsaka, K., Abe, H., and Yamamoto, K. (1998). DNS of Turbulent Heat Transfer in Channel Flow with Low to Medium-High Prandtl Number Fluid. *Int. J. Heat Fluid Flow* 19 (5), 482–491. doi:10.1016/s0142-727x(98)10026-7
- Kays, W. M. (1994). Turbulent Prandtl Number-Where Are We? *Asme Trans. J. Heat Transfer* 116 (2), 284–295. doi:10.1115/1.2911398
- Lai, Y. G., and So, R. M. C. (1990). Near-wall Modeling of Turbulent Heat Fluxes. *Int. J. Heat Mass Transfer* 33 (7), 1429–1440. doi:10.1016/0017-9310(90)90040-2
- Manservigi, S., and Menghini, F. (2014a). A CFD Four Parameter Heat Transfer Turbulence Model for Engineering Applications in Heavy Liquid Metals. *Int. J. Heat Mass Transfer* 69 (2), 312–326. doi:10.1016/j.jheatmasstransfer.2013.10.017
- Manservigi, S., and Menghini, F. (2015). CFD Simulations in Heavy Liquid Metal Flows for Square Lattice Bare Rod Bundle Geometries with a Four Parameter Heat Transfer Turbulence Model. *Nucl. Eng. Des.* 295 (12), 251–260. doi:10.1016/j.nucengdes.2015.10.006
- Manservigi, S., and Menghini, F. (2014b). Triangular Rod Bundle Simulations of a CFD $\kappa-\epsilon-\kappa-\epsilon$ Heat Transfer Turbulence Model for Heavy Liquid Metals. *Nucl. Eng. Des.* 273, 251–270. doi:10.1016/j.nucengdes.2014.03.022
- Mikityuk, K. (2009). Heat Transfer to Liquid Metal: Review of Data and Correlations for Tube Bundles. *Nucl. Eng. Des.* 239 (4), 680–687. doi:10.1016/j.nucengdes.2008.12.014
- Moukalled, F., Mangani, L., and Darwish, M. (2016). *The Finite Volume Method in Computational Fluid Dynamics*. Berlin: Springer International Publishing.
- Nagano, Y., Hattori, H., and Abe, K. (1997). Modeling the Turbulent Heat and Momentum Transfer in Flows under Different thermal Conditions. *Fluid Dyn. Res.* 20 (1-6), 127–142. doi:10.1016/s0169-5983(96)00049-4
- Nagano, Y., and Kim, C. (1988). A Two-Equation Model for Heat Transport in Wall Turbulent Shear Flows. *J. Heat Transfer* 110 (3), 583–589. doi:10.1115/1.3250532
- Nagano, Y., and Shimada, M. (1996). Development of a Two-equation Heat Transfer Model Based on Direct Simulations of Turbulent Flows with Different Prandtl Numbers. *Phys. Fluids* 8 (12), 3379–3402. doi:10.1063/1.869124
- Reynolds, A. J. (1975). The Prediction of Turbulent Prandtl and Schmidt Numbers. *Int. J. Heat Mass Transfer* 18 (9), 1055–1069. doi:10.1016/0017-9310(75)90223-9
- Schroer, C., Wedemeyer, O., Skrypnik, A., Novotny, J., and Konys, J. (2012). Corrosion Kinetics of Steel T91 in Flowing Oxygen-Containing lead–bismuth Eutectic at 450 °C. *J. Nucl. Mater.* 431 (1-3), 105–112. doi:10.1016/j.jnucmat.2011.11.014
- Shams, A., De Santis, A., and Roelofs, F. (2019). An Overview of the AHFM-NRG Formulations for the Accurate Prediction of Turbulent Flow and Heat Transfer in Low-Prandtl Number Flows. *Nucl. Eng. Des.* 355, 110342. doi:10.1016/j.nucengdes.2019.110342
- Shikazono, N., and Kasagi, N. (1996). Second-moment Closure for Turbulent Scalar Transport at Various Prandtl Numbers. *Int. J. Heat Mass Transfer* 39 (14), 2977–2987. doi:10.1016/0017-9310(95)00339-8
- Su, X. K., and Gu, L. (2021). *Numerical Study on Turbulent Heat Transfer of LBE in an Annulus Based on A Four-Equation Model*. Chinese Beijing: Atomic Energy Science and technology. Available at: <http://kns.cnki.net/kcms/detail/11.2044.TL.20210720.181>. doi:10.13832/j.jnpe.2021.S1.0026
- Su, X. K., Gu, L., Peng, T. J., Jiatai, L., Xianwen, L., and Guan, W. (2021). Research on a Four-Equation Model Based on OpenFOAM. *Nucl. Power Eng.* 42 (S1), 26–32. (in chinese).
- Subbotin, V. I., Ushakov, P. A., and Kirillov, P. L. (1965). “Heat Transfer in Elements of Reactors with a Liquid Metal Coolant,” in Proceedings of the 3rd International Conference on Peaceful Use of Nuclear Energy, Geneva, 192–200.
- Tiselj, L., and Cizelj, L. (2012). DNS of Turbulent Channel Flow with Conjugate Heat Transfer at Prandtl Number 0.01. *Nucl. Eng. Des.* 253 (1), 153–160. doi:10.1016/j.nucengdes.2012.08.008
- Wang, G., Gu, L., and Yun, D. (2021). Preliminary Multi-Physics Performance Analysis and Design Evaluation of UO₂ Fuel for LBE-Cooled Subcritical Reactor of China Initiative Accelerator Driven System. *Front. Energ. Res.* doi:10.3389/FENRG.202110.3389/fenrg.2021.732801
- Weller, H. G., Tabor, G., Jasak, H., and Fureby, C. (1998). A Tensorial Approach to Computational Continuum Mechanics Using Object-Oriented Techniques. *Comput. Phys.* 12 (6), 620–631. doi:10.1063/1.168744
- You, B. H., Jeong, Y. H., and Addad, Y. (2019). Assessment of Advanced RANS Models Ability to Predict a Turbulent Swept Liquid Metal Flow over a Wire in a Channel. *Nucl. Eng. Des.* 353 (Nov), 1102061–11020614. doi:10.1016/j.nucengdes.2019.110206
- Youssef, M. S. (2006). A Two-Equation Heat Transfer Model for wall Turbulent Shear Flows. *J. Eng. Sci.* 34 (6), 1877–1903. doi:10.21608/jesaun.2006.111184
- Zhukov, A. V., Kuzina, Y. A., Sorokin, A. P., Leonov, V. N., Smirnov, V. P., and Sila-Novitskii, A. G. (2002). An Experimental Study of Heat Transfer in the Core of a BREST-OD-300 Reactor with lead Cooling on Models. *Therm. Eng.* 49 (3), 175–184.

Conflict of Interest: The authors declare that the research was conducted in the absence of any commercial or financial relationships that could be construed as a potential conflict of interest.

Publisher’s Note: All claims expressed in this article are solely those of the authors and do not necessarily represent those of their affiliated organizations, or those of the publisher, the editors, and the reviewers. Any product that may be evaluated in this article, or claim that may be made by its manufacturer, is not guaranteed or endorsed by the publisher.

Copyright © 2022 Su, Li, Wang, Liu, Chen, Shi, Sheng and Gu. This is an open-access article distributed under the terms of the Creative Commons Attribution License (CC BY). The use, distribution or reproduction in other forums is permitted, provided the original author(s) and the copyright owner(s) are credited and that the original publication in this journal is cited, in accordance with accepted academic practice. No use, distribution or reproduction is permitted which does not comply with these terms.